APPENDIX A – Newman IFF Challenge Life Analyses using FASTRAN

QUESTIONNAIRE

Contact Name: A-10 Thunderbolt II and F-4 Phantom

Please provide information about the analyses completed:

1. Analysis Software (name and version)
    a. FEA software (if applicable): None
    b. Crack growth software: FASTRAN Version 5.70 [1]

2. Interference Fit Modeling
    a. Describe the methods used to characterize and incorporate the effect of the IFF.

        Because the tight interference-fit fastener (assuming friction) would greatly reduce the open-hole stress concentration and the stress distribution away from the hole would be nearly uniform stress. Thus, the crack-growth model was a simple "surface crack" with the same initial crack length (c_i) and initial crack depth (a_i) as the single corner crack at a hole. The different moduli from the plate and fastener were neglected. A finite-element analysis by Taghizadeh and Chalherlou (2017) [2] showed nearly uniform stress from an interference-fit fastener-hole analysis for a steel fastener in an aluminum alloy plate, similar to the current interference-fit problem.

    b. If the fastener effect was derived from a closed form solution, what were the assumptions of the solution. Is the solution based on empirical data or FEM correlations?

        The fastener effects (non-linear radial pressure distribution due to interference and variations during loading) were not considered because an initial surface crack in the plate (without a hole) was assumed. Based on some NASA work by Crews (1975) [3], the highest interference level (0.6% for a steel fastener in an aluminum plate) would not yield the hole during application.

3. Stress Intensity Calculations
    a. Describe the methods used to extract and calculate the stress intensities for applied remote loads.

Case 1: Single corner crack at an open hole under remote applied stress

Stress-intensity factor equations for a single corner crack at an open hole (1983) [4] were obtained from the Newman-Raju stress-intensity factor database. An improved stress-intensity factor equation for two-symmetric corner cracks at an open hole was updated using the more accurate Fawaz-Andersson (2000-2004) [5, 6] solutions for two-symmetric corner cracks at an open hole. The new equations are called the NRFA or modified NR (2005) [7] equations. In addition, an improved Shah [8] correction was recently developed to calculate the stress-intensity factor solution for a single corner crack at an open hole from the two-symmetric corner cracks at an open hole under remote tension using the more accurate Andersson-Fawaz (2017) [9] results.

For the single corner crack with an initial quarter circular shape (a/c = 1), the corner crack will grow faster along the bore of the hole than along the outer surface. Thus, some sample stress-intensity factor calculations have been made between the Andersson-Fawaz (2017) finite-element analysis tables and the NRFA (Newman-Raju-Fawaz-Andersson, 2005) with the improved Shah correction in Figure 1. Four cases are shown for difference a/c ratios as the crack grows through the thickness (a/t).

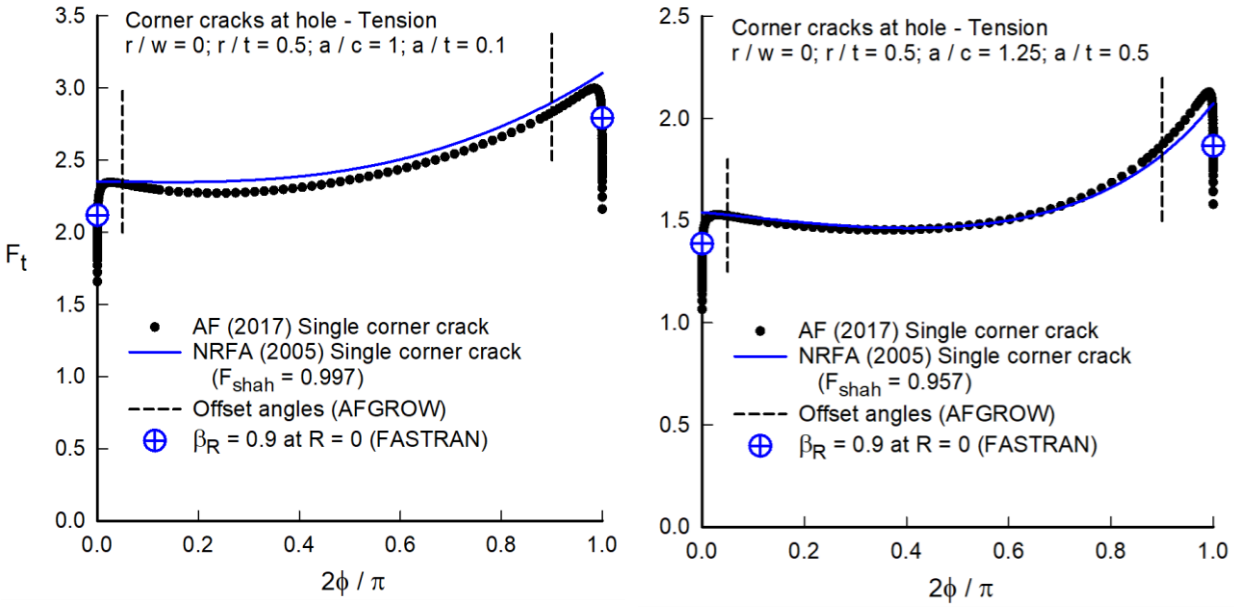

(a) a/c = 1.0 and a/t = 0.1 (b) a/c = 1.25 and a/t = 0.5

Figure 1(a) – Normalized stress-intensity factors for a single-corner crack at an open hole as a function of the parametric angle for small a/t ratios.

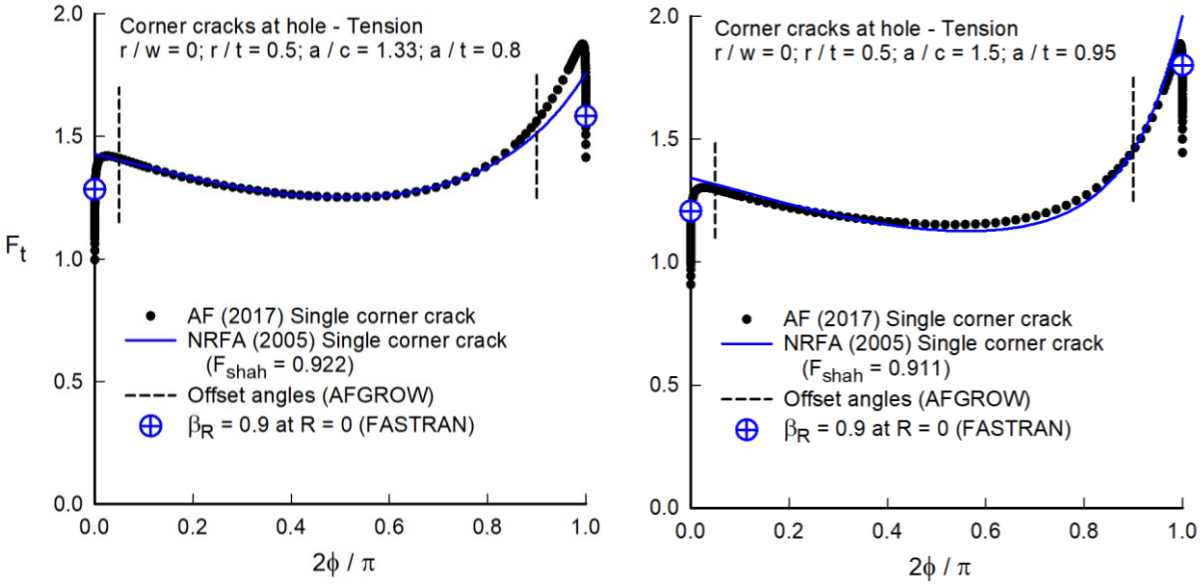

(a) a/c = 1.33 and a/t = 0.8 (b) a/c = 1.5 and a/t = 0.95

Figure 1(b) – Normalized stress-intensity factors for a single-corner crack at an open hole as a function of the parametric angle for very deep cracks.

The symbols are from the Anderson-Fawaz [9] tables and the curves are the NRFA equation with the modified Shah [8] conversion (converts the K-solution for two-symmetric corner cracks at an open hole to the K-solution for a single corner crack at open hole). The vertical dashed lines are the AFGROW offset angles (5 and 10 degrees) that are the K-value normally used in life predictions. (In a previous Challenge on cold-worked holes, some AFGROW users used the peak values and not the offset values. Not sure why this was done.) And the circle-cross symbols are the K-values used in the FASTRAN code for fatigue crack growth (plane-stress to plane-strain crack-closure correction). For R = 0 loading, β_R is 0.9, but for high R, β_R goes to unity as R = 1. The β_R factor [10] is used to help predict the crack shape and fatigue crack-growth lives. In all predictions, the corner crack is always assumed to be a quarter-elliptical shape.

Case 2 and 3: Interference-fit fasteners

Stress-intensity factor equations for the surface crack (1979) [11] were obtained from the Newman-Raju stress-intensity factor database. In reality, the corner crack at a filled hole looks like an offset surface crack, so the half-width (w) was selected as 1.075 in. and the initial surface-crack-depth and -length were the same as the initial corner-crack-depth and -length.

b. Describe the methods used to incorporate the stress intensities into the crack growth code (superposition, etc.)

For each case, an equation had previously been programed into the FASTRAN life-prediction code. Superposition was not used since the interference-fit fastener was assumed to make the plate material continuous with a surface crack assumed for the single corner crack at the hole. The difference in interference (0.4% and 0.6%) were neglected, and the initial crack length and initial crack depth were the same for both interference levels. Predicted life is expected to be somewhat conservative. In all cases, fatigue pre-cracking was simulated at the pre-cracking applied stress level and R value (same as applied in the IFF Challenge problems). An initial flaw shape and size was selected (close to the actual EDM values) that would produce the same crack length and depth stated as the starting crack size and shape for life predictions.

4. Crack Growth Predictions

   a. Describe the material model approach used for the crack growth predictions (NASGRO, tabular, etc.) and the assumptions/approach used for "threshold", stress ratio (R) shift, and negative R behavior.

There are two material models and two sets of predictions are made. One set is based on fatigue crack growth (ΔK-rate) data generated at MSU on C(T) specimens and compared with M(T) test data from the NASGRO database [12]. A ΔK_{eff}-rate curve was developed using the FASTRAN constraint-loss option (plane-strain to plane-stress behavior). This is called Data Set 1.

The other data set was obtained from the IFF Challenge supplied ΔK-rate data at only R = 0.1. A ΔK_{eff}-rate curve was developed using the FASTRAN model with a constant constraint factor of 2. This is called Data Set 2.

Data Set 1:

The crack-growth material model was based on Elber's Crack-Closure (ΔK_{eff}) Theory [13, 14]. The fatigue-crack-growth-rate equations are:

$$dc/dN = C_{1i1} (\Delta K_{eff1})^{C_{2i1}} [1 - (\Delta K_{o1}/\Delta K_{eff1})^{p}] / [1 - (K_{max1}/K_{Ie})^{q}] \qquad (1)$$

$$da/dN = C_{1i2} (\Delta K_{eff2})^{C_{2i2}} [1 - (\Delta K_{o2}/\Delta K_{eff2})^{p}] / [1 - (K_{max2}/K_{Ie})^{q}] \qquad (2)$$

where $\Delta K_{effj} = K_{maxj} - K_{op}$, C_{1ij} and C_{2ij} are multi-linear coefficients to fit several near linear sections along the ΔK_{effj}-rate data (j = 1 is c-direction and j = 2 is a-direction). See Figures 2(a) and 2(b) for rate data on the 7075-T651 aluminum alloy (different than that supplied in IFF Challenge). K_{op} is calculated from the FASTRAN (modified strip-yield) model for (1) cracks emanating from a circular hole or (2) a through crack in a plate, and K_{op} is assumed to be the same at the maximum depth and free-surface locations. Herein, the threshold term is

neglected ($\Delta K_{oj} = 0$). (The threshold term was originally developed to fit near-threshold test data that had been generated using the ASTM "load-shedding" method, but test data generated using the new compression pre-cracking methods showed that the threshold term was not needed for most materials. The current load-shedding method generates a load-history effect.) The fracture term was needed to model the crack-growth behavior as cracks grow to failure because, in general, non-linear Fracture Mechanics concepts are needed to predict fracture. Herein, the Two-Parameter Fracture Criterion (TPFC; K_F, m) [15] was used to predict K_{Ie}, the elastic stress-intensity factor at failure. K_F is the elastic-plastic fracture toughness and m is a fracture-toughness parameter that is m = 0 for brittle materials and m = 1 for very ductile materials. The K_{max} value is normalized by K_{Ie} (elastic stress-intensity factor at failure) and raised to the q power, which controls how rapid the fracture toughness is approached on a ΔK-rate relation. Failure occurs if the K_{max} value at either crack-depth or crack-length location reaches K_{Ie}.

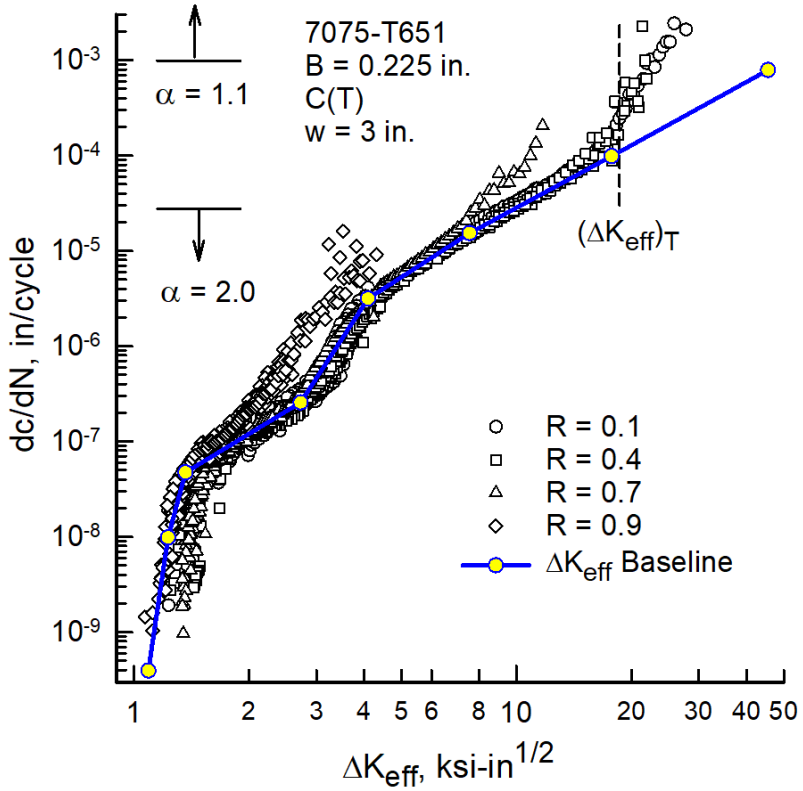

Figure 2(a) – Effective stress-intensity factor range against rate, dc/dN, over a wide range in rates and R value.

Figure 2(a) shows ΔK_{eff}-rate data on 7075-T651 (B = 0.225 in.) that was determined from ΔK-rate data generated on C(T) specimens over a wide range in R and rates from threshold to near fracture. The new compression pre-cracking procedures, CPCA – compression pre-cracking constant amplitude loading and CPLR – compression pre-cracking load reduction were used. The CPCA method generates test data with minimal load-history effects, but the CPLR method has been found to still have some load-history effects. However, the load-history effects are less than those found using the current ASTM E-647 test standard [16]. At high rates there is a constraint-loss behavior (α = 2 to 1.1) from plane-strain to plane-stress behavior [17]. For constant-amplitude loading, constraint loss is not a big issue. (Constraint-loss behavior is mainly needed for spectrum loading.) Lines (blue) with circular (yellow) symbols show the power-law term in Equation (1) for dc/dN.

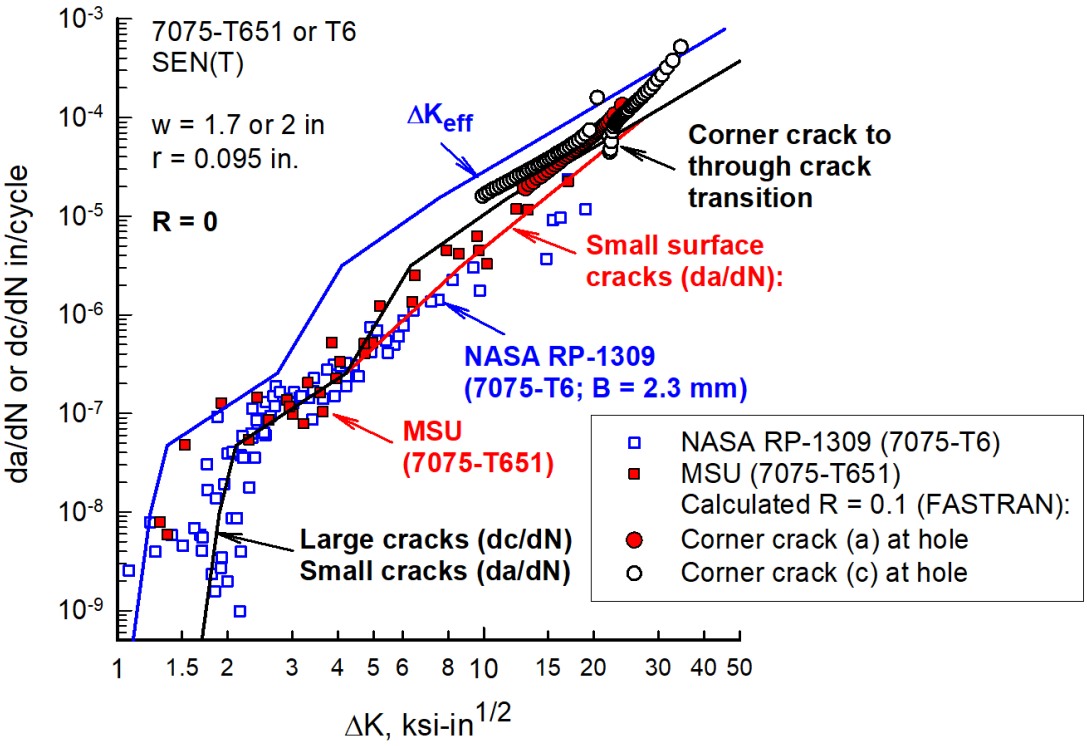

Figure 2(b) – Stress-intensity factor range against rate, da/dN and dc/dN, over a wide range in rates for small- and large-cracks in C(T), SEN(T) and corner-crack-at-open-hole specimens.

Figure 2(b) shows the ΔK-rate data for small cracks growing in the a-direction and the predicted behavior at R = 0. Small-crack data were obtained from SEN(T) specimens made of thin-sheet 7075-T6 [18] and thicker plate 7075-T651 [19]. Note that the shape transition at a rate of about 1.0e-6 in./cycle for the c-direction does not occur in the a-direction. This behavior is caused by the grain structure through the thickness as compared to the in-plane grain structure (grains are pancake-like in micro-structure). Lines (red) show the power-law

term in Equation (2) for da/dN. Here again, the threshold term was not used ($\Delta K_{o2} = 0$). The fracture term is used to predict how a crack in the open-hole case or IFF case grows to failure. The tabular data for Data Set 1 are given in Table 1 for Equations (1) and (2).

Table 1 – Data Set 1 material properties used in the FASTRAN code.

ΔK_{eff1} ksi-in$^{1/2}$	dc/dN (a) in./cycle	ΔK_{eff2} ksi-in$^{1/2}$	da/dN (a) in./cycle
1.0919	3.94E-10	1.0919	3.94E-10
1.2284	9.84E-09	1.2284	9.84E-09
1.3649	4.72E-08	1.3649	4.72E-08
2.7298	2.56E-07	2.7298	2.56E-07
4.0946	3.15E-06	5.6415	3.15E-06
7.5523	1.54E-05	17.743	9.84E-05
17.743	9.84E-05	---	---
45.496	7.87E-04	---	---
Constraint: $\alpha = 2$	$\leq$ 2.75E-05	$\alpha = 1.1$	$\geq$ 1.0E-03
Tensile:	$\sigma_{ys} = 73$ ksi	$\sigma_u = 84$ ksi	E = 10,400 ksi
Threshold:	$\Delta K_{o1} = 0$	$\Delta K_{o2} = 0$	p = 1
Fracture:	$K_F = 80$ ksi-in$^{1/2}$	m = 0.7	q = 2

(a) Crack growth rate in the a- and c-directions were different for a given ΔK_{eff}.

The open and solid circular symbols at high rates in Figure 2(b) show the calculated ΔK-rate data from the open-hole specimen predictions at R = 0.1. These data fall slightly higher than the R = 0 test data, as expected. A strange behavior occurred during the break-through (a/t = 1) condition. In the FASTRAN analysis, the K-solution at the maximum depth location gives a higher stress-intensity factor than a through crack of length, c. Thus, in the crack-closure analysis, the local K-solution acts like a slight overload that gives slower rates after breakthrough. Whether this happens in the open-hole test specimen under constant-amplitude loading will be seen in the IFF Challenge test data. (Of course, this can be changed by only allowing the free-surface K-solution to control the plasticity-induced closure model and not the average between the K-values at the 0 and 90-degree locations.)

In the previous Challenge problems, the majority of the fatigue crack-growth process was in the near-threshold regime, but in the current IFF Challenge case for the open-hole corner-crack configuration, all of the crack-growth rates occur in the constraint-loss regime ($\alpha = 2$ to 1.1), see Figures 2(a) and 2(b). The lower constraint ($\alpha \approx 1.7$) magnified the behavior from FASTRAN during the breakthrough (a/t = 1) conditions.

Data Set 2:

The crack-growth material model for Data Set 2 (see Fig. 3) was based on the R = 0.1 tabular ΔK-rate (triangular symbols) data provided in the IFF Challenge document. Because the open-hole single corner crack test and interference-fit (assume surface crack) tests were at R = 0.1, only the low-R data was used to develop the ΔK_{eff}-rate (blue) curve. The fatigue-crack-growth-rate equation is:

$$da/dN = dc/dN = C_{1i} (\Delta K_{eff})^{C_{2i}} \quad (3)$$

where $\Delta K_{eff} = K_{max} - K_{op}$, C_{1i} and C_{2i} are multi-linear coefficients to fit several near linear sections along the ΔK_{eff}-rate data, see Figure 3. K_{op} is calculated from the FASTRAN (modified strip-yield) model using a constraint factor of 2. (A constraint factor of 2 was found to collapse various sets of different R tests onto a nearly unique ΔK_{eff}-rate curve for 7000-series aluminum alloys.) The tabular data for Data Set 2 are given in Table 2 for Equation (3).

In Figure 3, the circular symbols show the calculated ΔK_{eff} values for the open-hole specimen with a single corner crack from FASTRAN; and the square symbols are the calculated ΔK values. The good agreement is a validation on input and output data from FASTRAN. Again, there was a small disturbance at the transition from a corner crack to a through crack (a/t = 1).

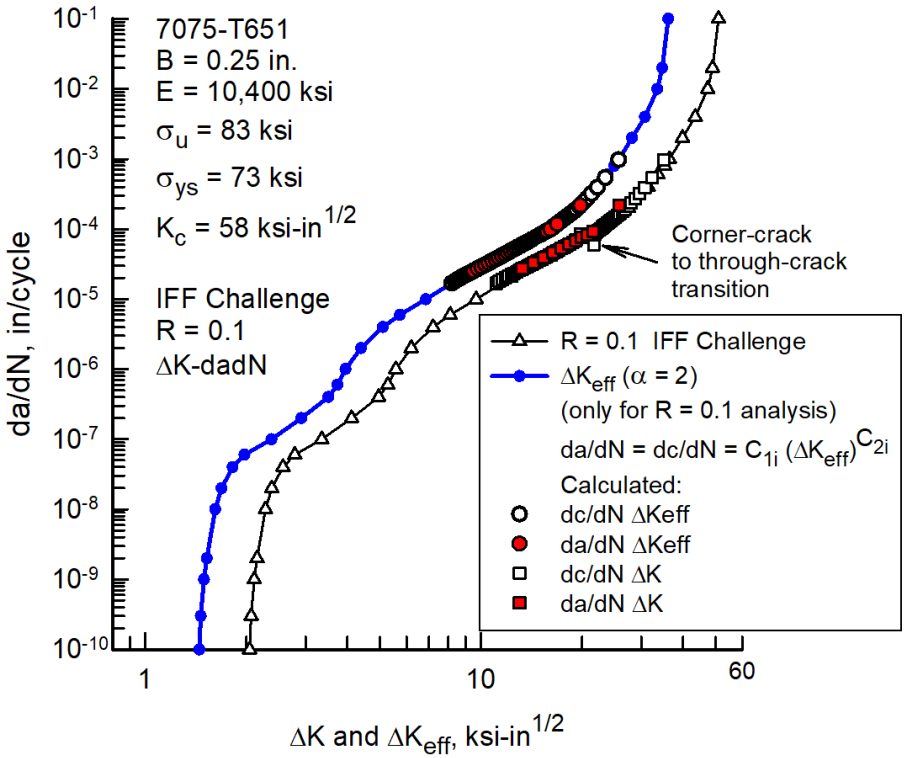

Figure 3 – Effective and normal stress-intensity factor range against rate, da/dN, over a wide range in rates and R = 0.1 from IFF Challenge test data.

Table 2 – Data Set 2 material properties.

ΔK_{eff} ksi-in$^{1/2}$	da/dN (a) in./cycle	ΔK_{eff} ksi-in$^{1/2}$	da/dN (a) in./cycle
1.425	1.00E-11	5.736	6.00E-06
1.448	1.00E-10	6.852	1.00E-05
1.462	3.00E-10	8.658	2.00E-05
1.495	1.00E-09	11.384	4.00E-05
1.524	2.00E-09	16.112	1.00E-04
1.615	1.00E-08	19.454	2.00E-04
1.686	2.00E-08	22.301	4.00E-04
1.82	4.00E-08	23.849	6.00E-04
1.974	6.00E-08	24.964	8.00E-04
2.375	1.00E-07	25.786	1.00E-03
2.914	2.00E-07	28.208	2.00E-03
3.509	4.00E-07	30.789	4.00E-03
3.736	6.00E-07	33.533	0.01
3.948	1.00E-06	34.666	0.02
4.391	2.00E-06	36.118	0.1
5.099	4.00E-06	---	---
Constraint:	α = 2	All rates	---
Tensile:	σ_{ys} = 73 ksi	σ_u = 83 ksi	E = 10,400 ksi
Fracture:	K_c = 58 ksi-in$^{1/2}$	---	---

(a) Crack growth rate in the a- and c-directions were assumed to be the same for a given ΔK_{eff}

Comparison of ΔK_{eff}-rate curves for Data Set 1 and 2:

A comparison between the ΔK_{eff}-rate curves for Data Set 1 and 2 are shown in Figure 4. The solid and dashed (black) curves with symbols are the curves used in FASTRAN to make crack growth predictions for the IFF Challenge. For Data Set 1, the constraint-loss (α = 2 to 1.1) option was used, as shown in the upper-rate region. The vertical dashed line shows the calculated flat-to-slant crack-growth location using $(\Delta K_{eff})_T$, the transition from plane-strain to plane-stress conditions [17], $(\Delta K_{eff})_T = 0.25\ (\sigma_{ys} + \sigma_u)\ \sqrt{(B)}$.

The solid (blue) curve is the curve developed from the IFF Challenge supplied crack growth rate data at R = 0.1 using a constant constraint factor of 2. In the low-rate regime, there are major differences (suspect that test data was generated using the ASTM load-shedding method, which has been shown to be flawed and causes a load-history effect on near-threshold data). The curves cross over in the high-rate regime and Data Set 2 go to fracture faster than that for Data Set 1. (Further study is needed on larger width test specimens to

generate better results in the high-rate regime. Need to separate the fracture regime from the constraint-loss regime.)

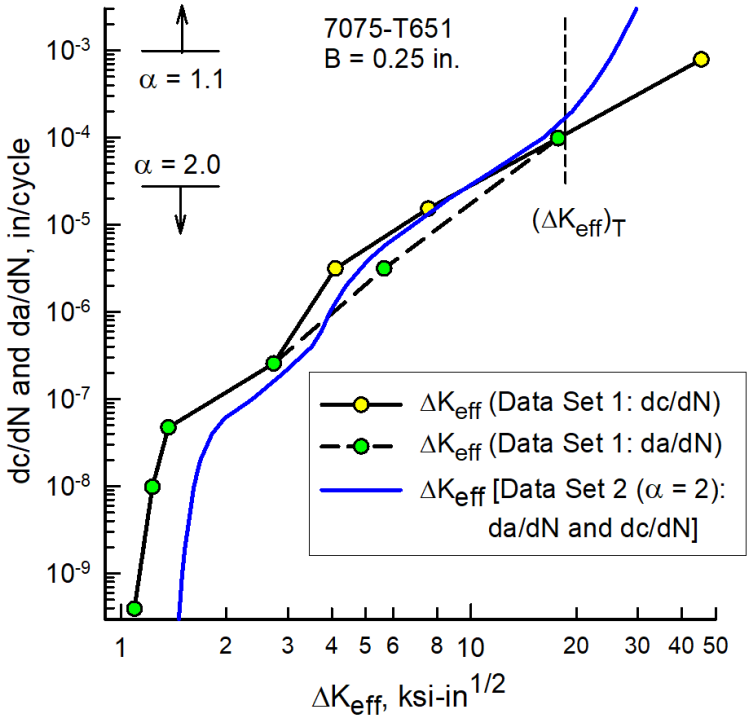

Figure 4 – Effective and normal stress-intensity factor range against rate, da/dN, over a wide range in rates and R = 0.1 from IFF Challenge test data

Comparison of Data Set 1 and 2 for open-hole single corner crack configuration:

A comparison between FASTRAN predictions for Data Set 1 and 2 for the single corner crack at an open hole specimen are shown in Figures 4 and 5. In Figure 4, the solid curves are crack length, c, against cycles, N; and the dashed curves are crack depth, a, against cycles. Black and blue curves are Data Set 1 and 2, respectively. There was about 17% difference in the fatigue crack growth lives. The model using Data Set 1 fractured at 48 ksi-in$^{1/2}$; while the model with Data Set 2 failed at 58 ksi-in$^{1/2}$. The difference was due to Data Set 1 using the TPFC that predicts the effects of width and crack length on the linear-elastic stress-intensity factor (K_{le}) at failure. (The FASTRAN code will be checked to see why the crack length, c_f, at failure was larger for Data Set 1 than Data Set 2.)

Figure 5 shows the predicted crack size (a/t) and shape (a/c) for the two models. Model for Data Set 2 grew the crack depth (a) faster than that for Data Set 1, because the model for Data Set 1 has slower crack-growth rates in the mid- to upper region than that for Data Set 2. The solid points indicate the a/t and a/c values where the comparisons were made on the stress-intensity factor solutions for a single corner crack at an open hole under uniform applied stress from Andersson-Fawaz [9] and Newman-Raju-Fawaz-Andersson equations [7].

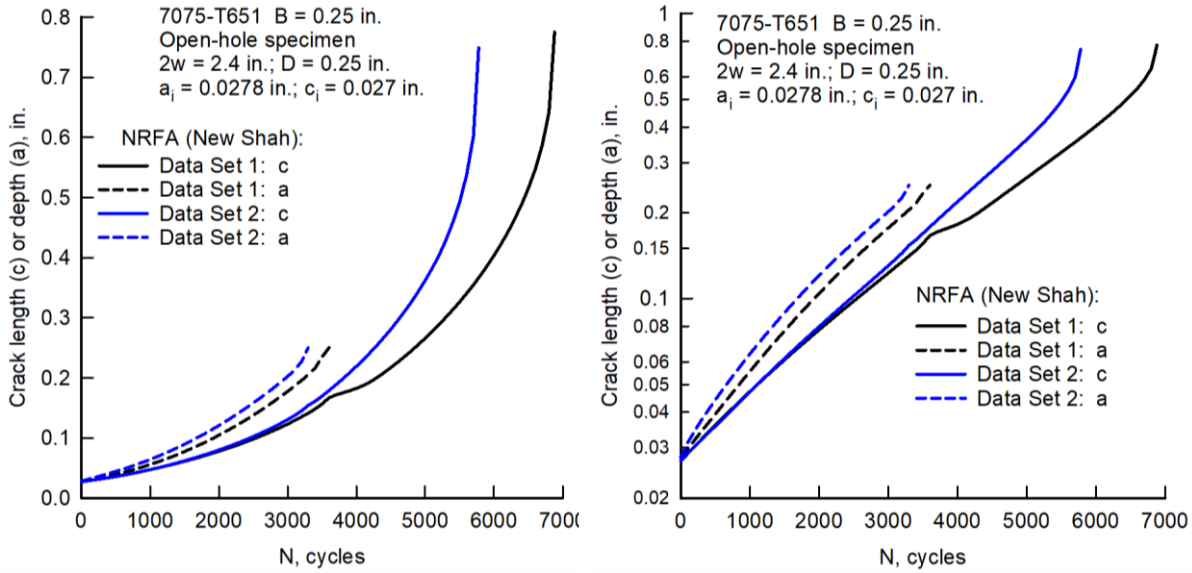

(a) Linear-linear crack length against cycles (b) Linear-log crack length against cycles

Figure 4 – Crack length and depth against cycles for single corner crack at open hole configuration at S_{max} = 27.9 ksi and R = 0.1.

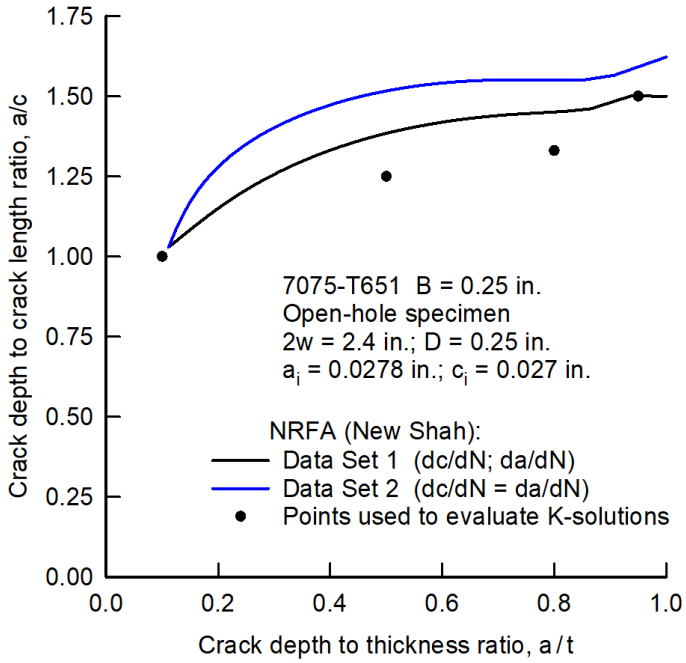

Figure 5 – Crack depth to length (a/c) ratio against crack depth to thickness (a/t) ratio for single corner crack at open hole configuration at S_{max} = 27.9 ksi and R = 0.1.

Comparison of Data Set 1 and 2 for IFF (surface crack) configuration:

Recall that the modeling of the Interference-Fit Fastener (IFF) was modeled as a simple offset surface crack in a plate. Thus, the two interference levels (0.4% and 0.6%) will result in the same predicted life to failure. It is estimated that this approach may result in a conservative life compared to the actual IFF tests.

A comparison between the FASTRAN predictions for Data Set 1 and 2 for the IFF cases (surface crack) are shown in Figures 6 and 7. In Figure 6, the solid curves are crack length, c, against cycles, N; and the dashed curves are crack depth, a, against cycles. The black and blue curves are Data Set 1 and 2, respectively. There was about 24% difference in the fatigue crack growth lives. The model using Data Set 1 fractured at 43 ksi-in$^{1/2}$; while the model with Data Set 2 failed at 58 ksi-in$^{1/2}$. The difference was due to Data Set 1 using the TPFC that predicts the effects of width and crack length on the linear-elastic stress-intensity factor (K_{Ie}) at failure. Thus, the specimen using Data Set 1 failed at a smaller crack length (c_f =0.53 in.) than that for Data Set 2 (c_f = 0.58 in.).

Figure 6(b) has plotted the predictions on a linear-log plot, which amplifies the results at the smaller crack sizes. When dealing with crack sizes that change by orders-of-magnitude, it is helpful to use a log scale to see the shape of the predicted curves in the early part of life.

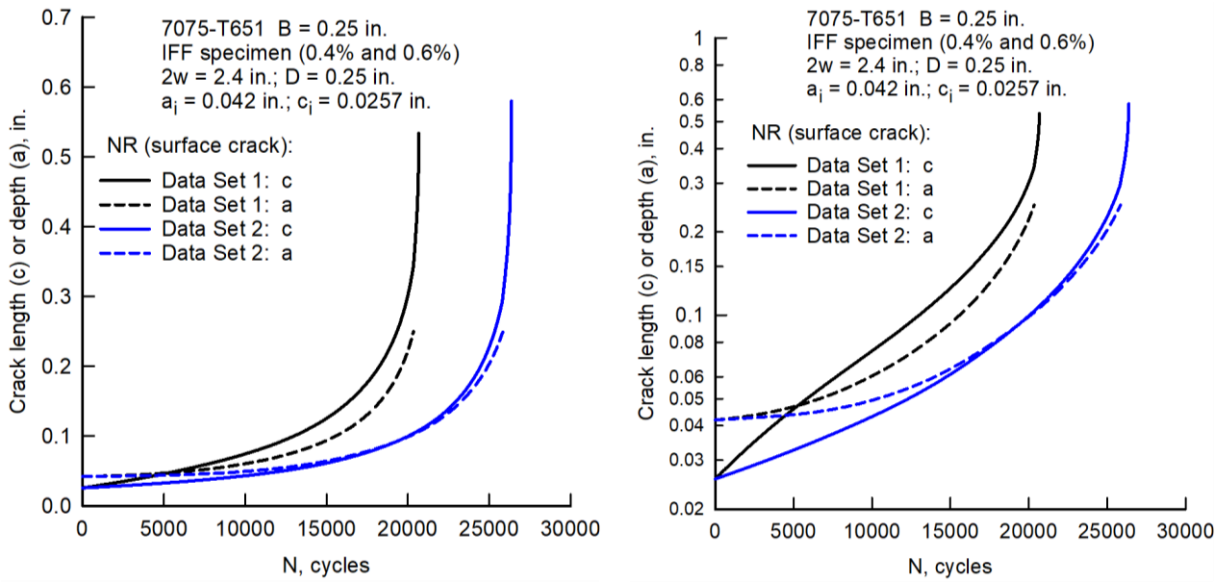

(a) Linear-linear crack length against cycles (b) Linear-log crack length against cycles

Figure 6 – Crack length and depth against cycles for IFF (surface crack) configuration at S_{max} = 27.9 ksi and R = 0.1.

Figure 7 shows the predicted crack size (a/t) and shape (a/c) for the two models. Model for Data Set 1 grew the crack length (c) faster than that for Data Set 1. In

contrast, the crack depth, a, grew faster than crack length, c, in the open-hole corner crack; while for the simulated surface crack for the IFF holes, crack length, c, grew faster than crack depth. Again, the log-linear plot (Fig. 7(b)) gives a better depiction of the changes in a/c with smaller a/t ratios.

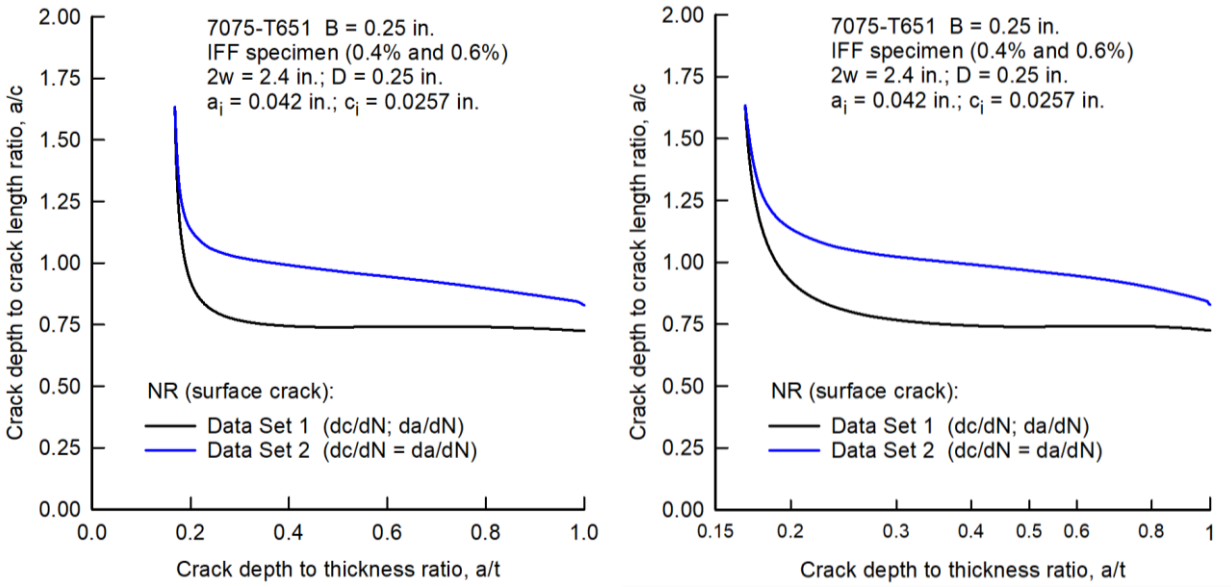

(a) Linear-linear a/c against a/t (b) Linear-log a/c against a/t

Figure 7 – Crack depth to length (a/c) ratio against crack depth to thickness (a/t) ratio for IFF (surface crack) configuration at S_{max} = 27.9 ksi and R = 0.1.

b. What growth increment was utilized between stress intensity calculations?

In all cases, the crack-growth increment was “cycle-by-cycle”. Execution times ranged from 5 to 40 seconds for all cases because of the high applied stress.

5. Provide any additional details that may be pertinent to the analyses completed

References below

References:

[1] Newman, J. C., Jr., FASTRAN—A Fatigue Crack Growth Life Prediction Code based on the Crack-Closure Concept, Version 5.4 User Guide, Fatigue and Fracture Associates, LLC, Eupora, MS, 2013.

[2] Taghizadeh, H. and Chalherlou, T. N., Experimental Investigation and Numerical Prediction of Fatigue Life in Force Fitted Fastener Holes, J Simulation & Analysis of Novel Technologies in Mechanical Engineering, Vol. 10(4), 2017, pp. 15-32.

[3] Crews, J. H., Jr., Analytical and Experimental Investigation of Fatigue in a Sheet Specimen with an Interference-Fit Bolt, NASA TN D-7926, July 1975.
[4] Newman, J. C., Jr. and Raju, I. S., Stress-Intensity Factor Equations for Cracks in Three-Dimensional Finite Bodies Subjected to Tension and Bending Loads. Computational Methods in the Mechanics of Fracture, S. N. Atluri, ed., Elsevier, 1986, pp. 311-334.
[5] Fawaz, S. A. and Andersson, B. "Accurate Stress Intensity Factor Solutions for Unsymmetric Corner Cracks at a Hole" Proceedings of Fourth Joint DoD/FAA/NASA Conference on Aging Aircraft, 15-18 May 2000, St. Louis, MO.
[6] Fawaz, S. A. and Andersson, B., "Accurate Stress Intensity Factor Solutions for Corner Cracks at a Hole," Engineering Fracture Mechanics, Vol. 71, No. 9-10, 2004.
[7] Newman, J. C., Jr., Evaluation of Structural Integrity Analysis Methodologies for Corrosion Prediction Models, Final Report, S&K Technologies, Inc., July 2005.
[8] Andersson, B., Private communication, 2020.
[9] Shah, R. C. "Stress-Intensity Factors for Through and Part-Through Cracks Originating at Fastener Holes," Mechanics of Crack Growth, ASTM 590, 1976, pp. 429-459.
[10] Newman, J. C., Jr. and Raju, I. S., Prediction of Fatigue Crack-Growth Patterns and Lives in Three-Dimensional Cracked Bodies. NASA TM-85787, 1984.
[11] Raju, I. S. and Newman, J. C., Jr., Stress-Intensity Factors for a Wide Range of Semi-Elliptical Surface Cracks in Finite-Thickness Plates. Engineering Fracture Mechanics, 11(4), 1979, pp. 817-829.
[12] Newman, J. C., Jr., Anagnostou, E. L., and D. Rusk, D., Fatigue and Crack-Growth Analyses on 7075-T651 Aluminum Alloy Coupons under Constant- and Variable-Amplitude Loading. International Journal of Fatigue, Vol. 62, 2014, pp. 133-143.
[13] Elber, W., Fatigue Crack Closure under Cyclic Tension. Engineering Fracture Mechanics, Vol. 2(1), 1970, pp. 37-45.
[14] Elber, W., The Significance of Fatigue Crack Closure, ASTM STP 486, 1971, pp. 230-242.
[15] Newman, J. C., Jr., Fracture Analysis of Surface- and Through-Cracked Sheets and Plates, Engineering Fracture Mechanics, Vol. 5, No. 3, 1973, pp. 667-689.
[16] Standard Test Method for Measurement of Fatigue Crack Growth Rates, ASTM E-647, 2012.
[17] Newman, J. C., Jr., Effects of Constraint on Crack Growth under Aircraft Spectrum Loading. Fatigue of Aircraft Materials, A. Beukers, T. deJong, J. Sinke, A. Vlot and L. B. Vogelesang, eds., 1992, pp. 83-109.
[18] Newman, J. C., Jr., Wu, X. R., Venneri, S. L. and Li, C. G., Small-Crack Effects in High-Strength Aluminum Alloys - A NASA/CAE Cooperative Program, NASA RP-1309, May 1994.
[19] Jordon, J.B., Bernard, J.D., and Newman, J.C., Jr., Quantifying Microstructurally Small Fatigue Crack Growth in an Aluminum Alloy using a Silicon-Rubber Replica Method, International Journal of Fatigue, Vol. 36, 2012, pp. 206-210.